Solar Physics (2023) 298:13
https://doi.org/10.1007/s11207-022-02106-1

# How Hot Can Small Solar Flares Get?

**Louise Harra[1,2] · Andrea F. Battaglia[3,2] · Krzysztof Barczynski[1,2] · Hannah Collier[3,2] · Säm Krucker[3,4] · Katharine K. Reeves[5] · George Doschek[6]**

Received: 6 October 2022 / Accepted: 29 December 2022 / Published online: 26 January 2023


**Abstract**
The temperature reached by solar flares is a key parameter to understanding the physical process that causes the energy release. In this work, we analysed data from a Hinode Observing Programme that focused on high cadence measurement of the flaring plasma. This was carried out when the X-ray imager and spectrometer (STIX) on Solar Orbiter was observing. We analysed 3 small microflares, and determined their evolution and temperature. The temperature of the B2.8 microflare reached 16 MK. There was evidence in the smaller B1.4 flare of Fe XXIV emission, indicating that hot plasma of 15 MK can be reached.

**Keywords** Flares · Corona

## 1. Introduction

Solar flares are fast releases of electromagnetic energy that can reach energies of $10^{32}$ ergs. They are categorised and measured in many different ways. One of the common methods is the flux observed in the soft X-ray range (0.1 – 0.8 nm) across the whole Sun. This is known as the GOES classification, and starts at the lowest "A" class flare ($< 10^{-7}$ W m$^{-2}$), and reaches the largest "X" ($> 10^{-4}$ W m$^{-2}$) class flare.

There is extensive interest in solar flares – from the extremely large events that are associated with space weather impacts at Earth, to small-scale flares (nanoflares and microflares) that may be associated with heating the corona, and forming the slow solar wind. At even more extremes of energies, stellar flares can release energies several orders of magnitude higher than the largest solar flare.

Studies have been carried out to understand the correlations between the wide range of energies measured, e.g. the emission measure (EM) and temperatures of flares. Feldman, Laming, and Doschek (1995) extrapolated this to the case of stellar flares, and found a consistent picture. Solar flares show this correlation over 4 orders of magnitude, and the stellar case takes it to a further 4 orders of magnitude in emission measure. This strong correlation over such a wide range of emission measures indicates a similar energy source. Shibata and Yokoyama (2002) presented a theory to explain this universal correlation between temperature and emission measure. Their theory is based on magnetic reconnection which includes heat conduction and chromospheric evaporation. With this model they predict the observed

G. Doschek is retired.

Extended author information available on the last page of the article

relationship EM $\propto B^{-5}\ T^{17/2}$, with B being the magnetic field strength (in Gauss). The temperature range where this is applicable is 6 MK to 100 MK.

In this paper we are particularly interested in the heating of small flares. So called "microflares" are often described as flares with GOES classification A, B or lower energies (Testa and Reale, 2020). Statistical studies were carried out using the Bragg Crystal Spectrometer (Culhane et al., 1991) onboard the Yohkoh mission (Ogawara et al., 1991) using X-ray spectral lines. Feldman et al. (1996) did an extensive study of 868 flares measuring their temperature, emission measure, and GOES classification. They found that major flares have a higher peak temperature than the weaker flares. Feldman, Doschek, and Behring (1996) also studied the weakest flares from A2 – A9 GOES classification, and found that their average temperature is around 5 MK.

There has been recent work on the temperatures reached during these small events. Testa and Reale (2020) analysed a microflare and found that it reaches $> 10$ MK at the start of the event and emission from an Fe XXIII line is observed, although weak. Measurements at the later phase of this event by Mitra-Kraev and Del Zanna (2019) found a peak lower temperature of only 4.5 MK. Differential emission measure calculations of a sub-A class flare using NuSTAR, Hinode/XRT, and SDO/AIA find a peak temperature of about 3 MK, with additional high-temperature emission up to 10 MK (Wright et al., 2017). Similar results were found for two additional sub-A class flares using a combination of the FOXSI-2 rocket, Hinode/XRT, and SDO/AIA (Athiray et al., 2020) instruments. The temperature reached during these small heating events is key for understanding the physical processes going on. These small flares occur much more frequently than their higher energy counterparts, e.g. Hudson (1991).

In 2020, the Solar Orbiter mission (Müller et al., 2020) was launched. The Spectrometer/Telescope for Imaging X-rays (STIX) has observed many thousands of small flares to date (see the STIX quicklook website: datacenter.stix.i4ds.net/view/plot/lightcurves). Battaglia et al. (2021) explores a range of microflares observed by STIX, and finds that at the lower energies they peak before the GOES intensity peak. This suggests that either STIX has a better sensitivity to higher temperatures than GOES, or these lower energies have a non-thermal component.

In this paper, we explore three microflares observed during a Hinode spacecraft (Kosugi et al., 2007) Observing Programme (HOP). This campaign was set up specifically to explore with high time cadence hot emission in flares. We have X-ray telescope data, Hinode EUV Imaging Spectrometer data (EIS) (Culhane et al., 2007), Solar Dynamics Observatory (SDO) Atmospheric Imaging Assembly (AIA) data (Pesnell, Thompson, and Chamberlin, 2012; Lemen et al., 2012), and STIX data (Krucker et al., 2020). These instruments provide multiple ways to access "hot" plasma to determine how hot a small flare can become.

## 2. Data Analysis

The data for this paper were obtained during a Hinode Observing Programme (HOP 361) concentrating on fast time cadence in active region NOAA12882. XRT provided data in one filter at a cadence of 10 sec using the Be_thin filter.

For EIS, the Fast_slot_hefe3 (study ID 544) was run. This is a 266″ slot entrance aperture with two channels – one for Fe XII and one for He II with 10 sec exposure times. We concentrated on the He II band in which the Fe XXIV emission line exists. Before and after this slot study was run, a large raster was carried out over the active region. The He II slot data covers a wavelength range of approximately 6 Å as shown in Harra et al. (2017). This

includes emission lines from Fe XXIV, S XIII, Fe XIV, and Si X. We are in this case particularly interested in the Fe XXIV emission, which has a temperature of 15 MK at maximum ion abundance. The method used to extract the Fe XXIV emission is described in Harra et al. (2020).

The key alignment for this work is between AIA and EIS to determine which features are spectral and which are dynamical changes on the Sun seen in imaging only. The SolarSoftWare routine aia_prep.pro is applied to the AIA data. The EIS slot data and AIA are aligned using the AIA 304 Å filter with the IDL solarsoft routine cross_corr.pro. This computes the cross-correlation function between the two images.

This campaign was carried out in coordination with Solar Orbiter. On this date, the spacecraft was at 0.67 AU, the angular separation between Earth and Solar Orbiter was 15.7 degrees. The time difference between the Sun–Earth and the Sun-Solar Orbiter was 162.7 sec. The STIX instrument was operating continuously during this time.

For the STIX spectroscopic analysis, the OSPEX forward fitting software of solar hard X-ray spectra has been used. In order to obtain temperature and emission measure, we fitted the spectra with the standard isothermal function '`vth`'. The package we employed for converting STIX data to a format readable by OSPEX is now included in the SSWIDL distribution. For more detailed corrections to be applied for each individual pixel and detector, the STIX pixel data (Krucker et al., 2020) at the highest cadence has been used. To reflect the early stage of the calibration, we added 5% systematic uncertainty in quadrature, which is currently (August 2022), the default value for the STIX data. For more details regarding the STIX spectral fitting, we refer to Battaglia et al. (2021).

During the observing period there were 3 microflares. The first was observed in GOES as a B2.8 ($2.8 \times 10^{-7}$ W m$^{-2}$) flare (non-background subtracted). The second was smaller at B1.8 and the third was barely registered above the background in GOES, which was approximately at $1.4 \times 10^{-7}$ W m$^{-2}$. The high energy GOES band (0.5- 4 Å) was too weak to carry out a temperature analysis from GOES for any of the flares analysed.

## 3. Results

Figure 1 shows the active region as observed by XRT before and during the first and second flares. The source of the highest intensity is a small compact source. Multiple peaks were observed during this first flare, lasting 10 minutes. The next two flares seen by XRT were a factor of 6 smaller. These flares were seen by XRT, very weakly by EIS, but not by STIX. This observation in itself indicates that the temperatures of the later flares were lower than for the first flare.

Figure 2 shows the temporal evolution of the brightest source of the flares from both AIA and the EIS slot data using a stack plot. We use both AIA (304 Å) and EIS in this figure to highlight the imaging features and the spectral features. AIA enhancements show spatial changes only, whereas EIS slot enhancements show spatial and spectral changes. This analysis allows for the extraction of intensity in different emission lines at a fast time cadence in EIS. When there are enhancements in the emission lines in the EIS slot data, they are visible along the $y$-axes in Figure 2. The S XIII, Fe XIV, and Si X wavelengths are all longer than that of the He II at 256.32 Å and hence their enhancements are seen below the bright feature in the figure. We are particularly interested in Fe XXIV as the hottest emission line in this wavelength range, which is at 255.11 Å sitting above He II in the figure. To determine the wavelength scale, we assumed the peak of the EIS intensity was at

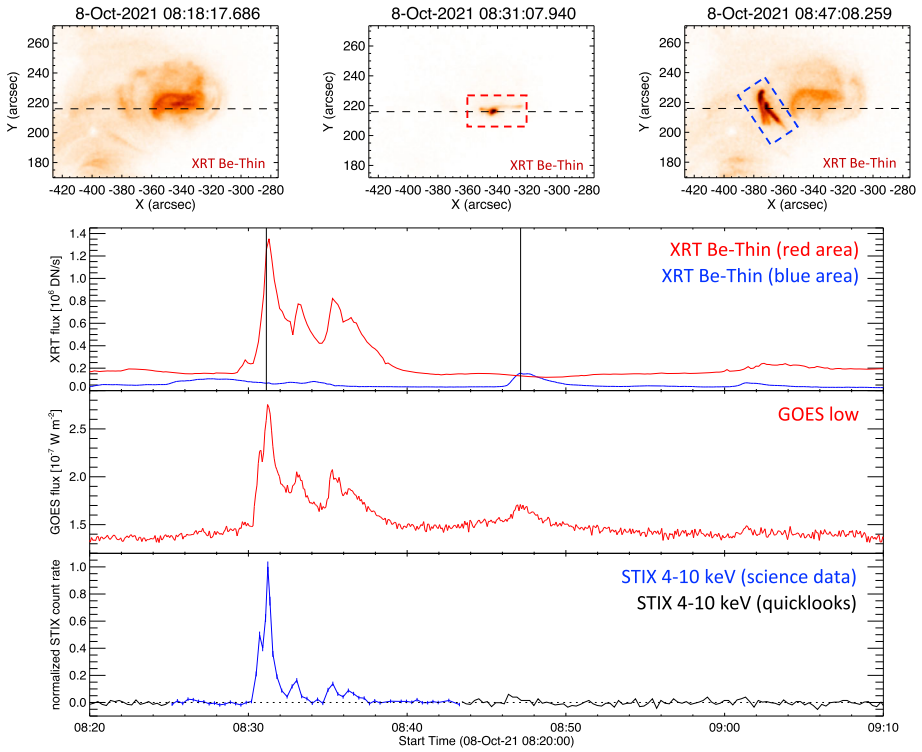


**Figure 1** The top figures show images of the active region before and during the first and second flare in our observing sequence. Note that the exposure time during the main flare is much shorter (0.045 sec) than for the image before the background (1.4 sec) and the active region is therefore not visible during the flare. For the weaker second flare, the exposure time is 0.594 sec and the active region is visible. Note that the first and second flare are clearly spatially separated. Below, X-ray time profiles from XRT, GOES and STIX are shown (the black vertical lines mark the times of the two XRT images with flaring activity shown above). The horizontal line marks the position y = 216″ from which later stack plots are determined. The STIX lightcurve gives the emission at 4 – 10 keV, where the blue section denotes science data and the black lightcurve is the low-latency ("quicklook") data. For GOES and STIX, the solar disk integrated flux is shown, while for XRT time profiles give the summed flux over the two flaring regions, marked in blue and red in the images shown on the top. The second smaller flares (08:47 UT and 09:02 UT) are barely discernible above the background in STIX and GOES.

the He II line at 256.32 Å. This line is the strongest emission line in this range and hence the assumption is a good one.

The first flare, starting at 08:30 UT, shows this spectral dispersion clearly. There are additional bright features seen along the *y*-axes (wavelength range) that cannot be seen by the imager AIA. From this stack plot, we can then extract lightcurves at different wavelengths and compare them with different energy lightcurves. Figure 3 illustrates the lightcurve comparison between the EIS slot intensity at the He II emission line, and the STIX 5 – 12 keV energy range for the first flare. The He II lightcurve shows an enhancement and starts to rise earlier than the STIX data. However, the STIX data peaks before the largest peak in the EIS He II data, which shows the largest peak at 08:32 UT. The EIS Fe XXIV peak is at the same time as the STIX peak.

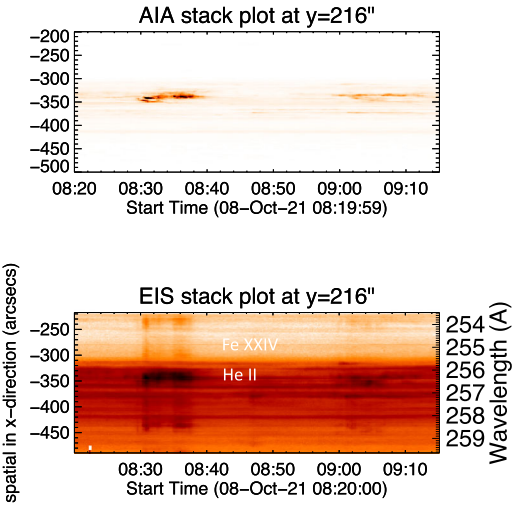


**Figure 2** The top plot is an AIA 304 Å stack plot chosen at y = 216″. This position in EIS exhibited the highest intensity during the flare. The stack plot shows the X-direction on the $y$-axes and time on the $x$-axes. The first flare with the multiple peaks is clearly seen starting at approximately 08:30 UT. The small flare starting at 09:02 UT is also clearly seen. The lower plot is the same figure, but for the EIS slot data. In this case, the $x$-direction is a mixture of wavelength and spatial information, and hence the wavelength scale is shown. There are additional features along the $y$-axes that emerge during the flare that are not seen in AIA – these are spectral features. The intensity is plotted in a log scale to highlight the additional spectral features. Of particular interest is any evidence of enhanced emission at 255.11 Å which is the Fe XXIV emission line.

The first flare shows a very compact structure, as is seen in Figure 4. The flare region covers just over 5 ″ in the $x$- and $y$-directions. The AIA 1600 Å image is shown with sources from EIS, XRT, and STIX overlaid. The source is so small that the STIX source lies over all features as a single source. The images were taken at the start of the first flare.

We are particularly interested in the temperature of small flares. Emission was seen in different energy bands up to 16 keV with STIX, allowing the temperature to be calculated. Figure 5 shows the STIX background-subtracted count flux spectrum at the peak intensity. An isothermal model, from the CHIANTI database, has been fitted to the data (reduced $\chi^2 = 2.7$ with 6 degrees of freedom), which, by assuming coronal abundances, results in a temperature of $15.9 \pm 0.8$ MK and an emission measure of $(1.0 \pm 0.3) \times 10^{46}$ cm$^{-3}$.

Using the temperature and emission measure derived from the STIX spectrum in Figure 5, we calculate the expected flux in the XRT Be-thin filter as a check. We find that a temperature of 15.9 MK and a volume emission measure of $10^{49}$ cm$^{-3}$ yields a count rate of about 42750 DN s$^{-1}$, assuming photospheric abundances. The brightest pixel in the XRT Thin-Be channel for the first flare occurs at 08:31:07 UT, and has a value of 41690 DN s$^{-1}$, remarkably close to the predicted value. This result indicates that 15.9 MK is a good estimate for the temperature in this flare.

We then looked at the EIS data to explore whether there was evidence for Fe XXIV emission, which has a temperature of maximum abundance of 15 MK. This value is very close to the temperature determined from STIX. Figure 6 shows lightcurves for the EIS Fe XXIV 255.11 Å line and the EIS He II line, for the time period of all three flares. The first larger flare is seen clearly at both the He II and Fe XXIV wavelengths. There are two peaks seen in the Fe XXIV, whereas only one peak is seen in the STIX data in Figure 3. The two smaller flares that follow at 08:47 UT and 09:02 UT are seen in the He II data. The flare at

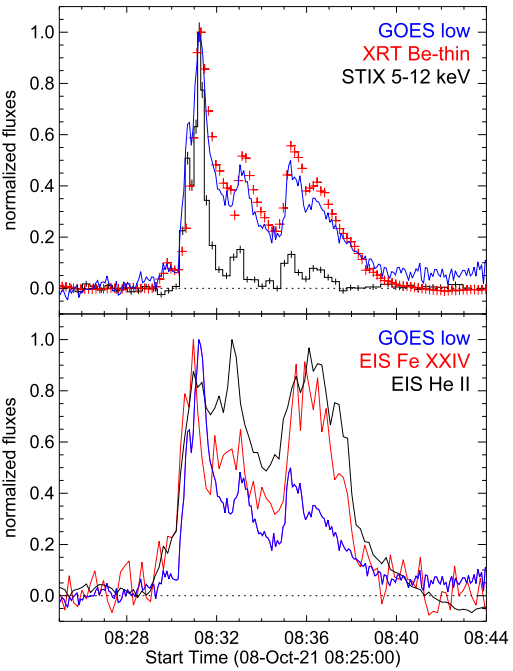


**Figure 3** The top figure shows the lightcurves in X-rays from GOES, XRT, and STIX for the first flare. Below the lightcurves derived from the stack plot at the He II and the Fe XXIV emission line are given. For reference, the GOES lightcurve is shown in both panels. Multiple peaks are seen. The EIS Fe XXIV at 255.11 Å and He II at 256.32 Å lightcurves are derived from Figure 2, where the wavelength is chosen along the $y$-axis (the spectral direction) shown in Figure 2.

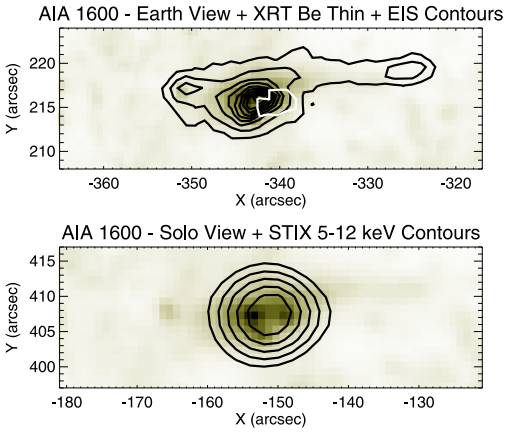


**Figure 4** The top panel shows an AIA 1600 Å image at 08:30:39 UT, around the first flare site. The black contours show the XRT Be Thin image taken at 08:31:07 UT, with contours levels 20 – 90% in 10% increments. The white 90% contour shows the EIS image taken at 08:30:34 UT. The bottom panel shows the AIA 1600 Å image reprojected to the Solar Orbiter viewpoint. The STIX 5 – 12 keV thermal emission is shown in black contours with levels 50 – 90% in 10% increments. The contours have been manually aligned to AIA 1600 Å with a shift of $\Delta x = -6''$, $\Delta y = +6''$, which is within the accuracy of the current implementation of the STIX aspect system.

08:47 UT has a very small enhancement above the background in EIS. The flare at 09:02 UT is clearly seen in He II. The flare at 08:47 UT does not show a significant enhancement above the background at the Fe XXIV wavelength, and there is an enhancement seen for the

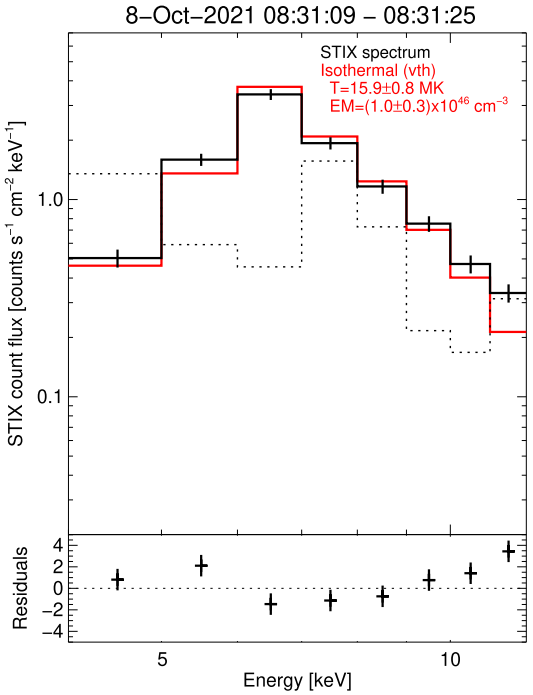


**Figure 5** STIX background subtracted count flux spectrum at the peak intensity. The observed spectrum has been fitted with an isothermal model (red curve), resulting in a temperature of 15.9 ± 0.8 MK. The black dashed line represents the non-solar background, which is dominated by the onboard calibration source. Below the spectrum plot, we show the residuals, i.e., observations minus fit, normalised by the errors.

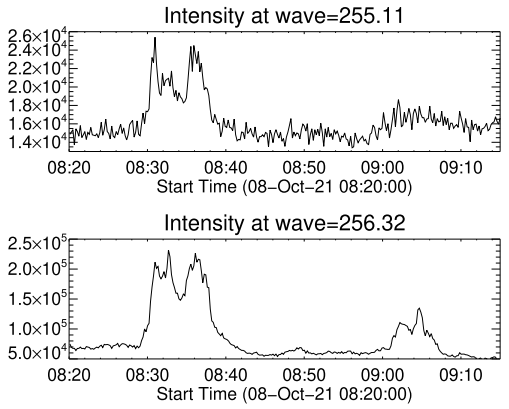


**Figure 6** The top figure shows the lightcurve derived from the EIS stack plot at the Fe XXIV wavelength, and the lower plot shows the lightcurve for the He II wavelength.

flare starting at 09:02 UT, which reaches 10% above the background in intensity. Neither of the second smaller flares are seen in STIX.

A Differential Emission Measure (DEM) was determined from AIA during these flares. There was an issue with saturated pixels, which meant that the calculation unfortunately had to exclude the flare site, so a temperature of the flare region could not be determined. The surrounding regions of the flare were at a temperature of around 2 MK.

## 4. Conclusions

We explored the temperature of a series of small flares observing with Hinode, STIX, and SDO. The largest flare in our series was a B2.8 flare (on top of a B1.5 pre-flare background), so a microflare. It is well known that flare plasma is multi-thermal, and this is seen clearly here with a range of temperatures observed. The first flare was observed with all the instruments. A temperature of $15.9 \pm 0.8$ MK was observed at the peak of the flare by STIX, and evidence of Fe XXIV emission confirmed this. In addition, cooler emission at He II existed alongside all the filters in AIA – confirming that there is a multi-thermal plasma.

The smaller flares that followed, which barely registered in GOES, were not seen by STIX. This observation provides an upper limit of the flare classification of approximately B2 GOES level. The last flare did show some very weak emission in the Fe XXIV wavelength, so even at this low intensity level there is some evidence of plasma reaching 15 MK. The temperatures observed in this work are consistent with the hot temperatures also seen by Testa and Reale (2020) during a small flare. They observed temperature $> 10$ MK. In addition, in the statistical work of Feldman et al. (1996), they found that flares with temperatures of 15 MK ranged from greater than B6 to M1 GOES classification. In the Feldman, Doschek, and Behring (1996) study of very small flares, the average temperature was 5 MK, but an A4 flare reached a temperature of 9 MK. NuSTAR observations of GOES A-class flares show temperatures from 6 MK up to 10 MK (Glesener et al., 2020; Duncan et al., 2021) for GOES A-class flares, while Glesener et al. (2017) reported temperatures between 6 and 8 MK for a sub-A-class flare.

Accurately determining how hot plasma can become during these small flares has implications for coronal heating (e.g Klimchuk 2006, Fletcher et al. 2015) as well as for flare physics. Processes such as magnetic reconnection are thought to be significant in both small and large scale flares. Cargill, Bradshaw, and Klimchuk (2012) developed a model to track the thermal evolution of loops due to small impulsive heating events, and in the distribution of emission measure with temperature there is a component at about 10 MK. This is difficult to measure as it is often so weak, but this work illustrates that high time cadence measurements of hot plasma observations can be made from spectroheliogram data of the weakest flares, and that these can show hot plasma.

**Author contributions** Harra wrote the main manuscript and analysed the EIS/XRT data. Battaglia, Collier, and Krucker worked on the STIX and combined datasets and text. Reeves worked on the XRT data and text. Doschek worked on the text.

**Funding Note** Open access funding provided by Swiss Federal Institute of Technology Zurich.

## Declarations

**Competing interests** The authors declare no competing interests.

## References


Athiray, P.S., Vievering, J., Glesener, L., Ishikawa, S.-n., Narukage, N., Buitrago-Casas, J.C., Musset, S., Inglis, A., Christe, S., Krucker, S., Ryan, D.: 2020, FOXSI-2 solar microflares. I. Multi-instrument differential emission measure analysis and thermal energies. *Astrophys. J.* **891**, 78. DOI. ADS.

Battaglia, A.F., Saqri, J., Massa, P., Perracchione, E., Dickson, E.C.M., Xiao, H., Veronig, A.M., Warmuth, A., Battaglia, M., Hurford, G.J., Meuris, A., Limousin, O., Etesi, L., Maloney, S.A., Schwartz, R.A., Kuhar, M., Schuller, F., Senthamizh Pavai, V., Musset, S., Ryan, D.F., Kleint, L., Piana, M., Massone, A.M., Benvenuto, F., Sylwester, J., Litwicka, M., Stęślicki, M., Mrozek, T., Vilmer, N., Fárník, F., Kašparová, J., Mann, G., Gallagher, P.T., Dennis, B.R., Csillaghy, A., Benz, A.O., Krucker, S.: 2021, STIX X-ray microflare observations during the Solar Orbiter commissioning phase. *Astron. Astrophys.* **656**, A4. DOI. ADS.

Cargill, P.J., Bradshaw, S.J., Klimchuk, J.A.: 2012, Enthalpy-based thermal evolution of loops. II. Improvements to the model. *Astrophys. J.* **752**, 161. DOI. ADS.

Culhane, J.L., Hiei, E., Doschek, G.A., Cruise, A.M., Ogawara, Y., Uchida, Y., Bentley, R.D., Brown, C.M., Lang, J., Watanabe, T., Bowles, J.A., Deslattes, R.D., Feldman, U., Fludra, A., Guttridge, P., Henins, A., Lapington, J., Magraw, J., Mariska, J.T., Payne, J., Phillips, K.J.H., Sheather, P., Slater, K., Tanaka, K., Towndrow, E., Trow, M.W., Yamaguchi, A.: 1991, The Bragg crystal spectrometer for SOLAR-A. *Solar Phys.* **136**, 89. DOI. ADS.

Culhane, J.L., Harra, L.K., James, A.M., Al-Janabi, K., Bradley, L.J., Chaudry, R.A., Rees, K., Tandy, J.A., Thomas, P., Whillock, M.C.R., Winter, B., Doschek, G.A., Korendyke, C.M., Brown, C.M., Myers, S., Mariska, J., Seely, J., Lang, J., Kent, B.J., Shaughnessy, B.M., Young, P.R., Simnett, G.M., Castelli, C.M., Mahmoud, S., Mapson-Menard, H., Probyn, B.J., Thomas, R.J., Davila, J., Dere, K., Windt, D., Shea, J., Hagood, R., Moye, R., Hara, H., Watanabe, T., Matsuzaki, K., Kosugi, T., Hansteen, V., Wikstol, Ø.: 2007, The EUV imaging spectrometer for Hinode. *Solar Phys.* **243**, 19. DOI. ADS.

Duncan, J., Glesener, L., Grefenstette, B.W., Vievering, J., Hannah, I.G., Smith, D.M., Krucker, S., White, S.M., Hudson, H.: 2021, NuSTAR observation of energy release in 11 solar microflares. *Astrophys. J.* **908**, 29. DOI. ADS.

Feldman, U., Doschek, G.A., Behring, W.E.: 1996, Electron temperature and emission measure determinations of very faint solar flares. *Astrophys. J.* **461**, 465. DOI. ADS.

Feldman, U., Laming, J.M., Doschek, G.A.: 1995, The correlation of solar flare temperature and emission measure extrapolated to the case of stellar flares. *Astrophys. J. Lett.* **451**, L79. DOI. ADS.

Feldman, U., Doschek, G.A., Behring, W.E., Phillips, K.J.H.: 1996, Electron temperature, emission measure, and X-ray flux in A2 to X2 X-ray class solar flares. *Astrophys. J.* **460**, 1034. DOI. ADS.

Fletcher, L., Cargill, P.J., Antiochos, S.K., Gudiksen, B.V.: 2015, Structures in the outer solar atmosphere. *Space Sci. Rev.* **188**, 211. DOI. ADS.

Glesener, L., Krucker, S., Hannah, I.G., Hudson, H., Grefenstette, B.W., White, S.M., Smith, D.M., Marsh, A.J.: 2017, NuSTAR hard X-ray observation of a sub-a class solar flare. *Astrophys. J.* **845**, 122. DOI. ADS.

Glesener, L., Krucker, S., Duncan, J., Hannah, I.G., Grefenstette, B.W., Chen, B., Smith, D.M., White, S.M., Hudson, H.: 2020, Accelerated electrons observed down to $< 7$ keV in a NuSTAR solar microflare. *Astrophys. J. Lett.* **891**, L34. DOI. ADS.

Harra, L.K., Hara, H., Doschek, G.A., Matthews, S., Warren, H., Culhane, J.L., Woods, M.M.: 2017, Measuring velocities in the early stage of an eruption: using "overlappogram" data from Hinode EIS. *Astrophys. J.* **842**, 58. DOI. ADS.

Harra, L., Matthews, S., Long, D., Hasegawa, T., Lee, K.-S., Reeves, K.K., Shimizu, T., Hara, H., Woods, M.: 2020, Locating hot plasma in small flares using spectroscopic overlappogram data from the Hinode EUV imaging spectrometer. *Solar Phys.* **295**, 34. DOI. ADS.

Hudson, H.S.: 1991, Solar flares, microflares, nanoflares, and coronal heating. *Solar Phys.* **133**, 357. DOI. ADS.

Klimchuk, J.A.: 2006, On solving the coronal heating problem. *Solar Phys.* **234**, 41. DOI. ADS.

Kosugi, T., Matsuzaki, K., Sakao, T., Shimizu, T., Sone, Y., Tachikawa, S., Hashimoto, T., Minesugi, K., Ohnishi, A., Yamada, T., Tsuneta, S., Hara, H., Ichimoto, K., Suematsu, Y., Shimojo, M., Watanabe, T., Shimada, S., Davis, J.M., Hill, L.D., Owens, J.K., Title, A.M., Culhane, J.L., Harra, L.K., Doschek, G.A., Golub, L.: 2007, The Hinode (Solar-B) mission: an overview. *Solar Phys.* **243**, 3. DOI. ADS.

Krucker, S., Hurford, G.J., Grimm, O., Kögl, S., Gröbelbauer, H.-P., Etesi, L., Casadei, D., Csillaghy, A., Benz, A.O., Arnold, N.G., Molendini, F., Orleanski, P., Schori, D., Xiao, H., Kuhar, M., Hochmuth, N., Felix, S., Schramka, F., Marcin, S., Kobler, S., Iseli, L., Dreier, M., Wiehl, H.J., Kleint, L., Battaglia, M., Lastufka, E., Sathiapal, H., Lapadula, K., Bednarzik, M., Birrer, G., Stutz, S., Wild, C., Marone, F., Skup, K.R., Cichocki, A., Ber, K., Rutkowski, K., Bujwan, W., Juchnikowski, G., Winkler, M., Darmetko, M., Michalska, M., Seweryn, K., Białek, A., Osica, P., Sylwester, J., Kowalinski, M., Ścisłowski, D.,

Siarkowski, M., Stęślicki, M., Mrozek, T., Podgórski, P., Meuris, A., Limousin, O., Gevin, O., Le Mer, I., Brun, S., Strugarek, A., Vilmer, N., Musset, S., Maksimović, M., Fárník, F., Kozáček, Z., Kašparová, J., Mann, G., Önel, H., Warmuth, A., Rendtel, J., Anderson, J., Bauer, S., Dionies, F., Paschke, J., Plüschke, D., Woche, M., Schuller, F., Veronig, A.M., Dickson, E.C.M., Gallagher, P.T., Maloney, S.A., Bloomfield, D.S., Piana, M., Massone, A.M., Benvenuto, F., Massa, P., Schwartz, R.A., Dennis, B.R., van Beek, H.F., Rodríguez-Pacheco, J., Lin, R.P.: 2020, The spectrometer/telescope for imaging X-rays (STIX). *Astron. Astrophys.* **642**, A15. DOI. ADS.

Lemen, J.R., Title, A.M., Akin, D.J., Boerner, P.F., Chou, C., Drake, J.F., Duncan, D.W., Edwards, C.G., Friedlaender, F.M., Heyman, G.F., Hurlburt, N.E., Katz, N.L., Kushner, G.D., Levay, M., Lindgren, R.W., Mathur, D.P., McFeaters, E.L., Mitchell, S., Rehse, R.A., Schrijver, C.J., Springer, L.A., Stern, R.A., Tarbell, T.D., Wuelser, J.-P., Wolfson, C.J., Yanari, C., Bookbinder, J.A., Cheimets, P.N., Caldwell, D., Deluca, E.E., Gates, R., Golub, L., Park, S., Podgorski, W.A., Bush, R.I., Scherrer, P.H., Gummin, M.A., Smith, P., Auker, G., Jerram, P., Pool, P., Soufli, R., Windt, D.L., Beardsley, S., Clapp, M., Lang, J., Waltham, N.: 2012, The Atmospheric Imaging Assembly (AIA) on the Solar Dynamics Observatory (SDO). *Solar Phys.* **275**, 17. DOI. ADS.

Mitra-Kraev, U., Del Zanna, G.: 2019, Solar microflares: a case study on temperatures and the Fe XVIII emission. *Astron. Astrophys.* **628**, A134. DOI. ADS.

Müller, D., St. Cyr, O.C., Zouganelis, I., Gilbert, H.R., Marsden, R., Nieves-Chinchilla, T., Antonucci, E., Auchère, F., Berghmans, D., Horbury, T.S., Howard, R.A., Krucker, S., Maksimovic, M., Owen, C.J., Rochus, P., Rodriguez-Pacheco, J., Romoli, M., Solanki, S.K., Bruno, R., Carlsson, M., Fludra, A., Harra, L., Hassler, D.M., Livi, S., Louarn, P., Peter, H., Schühle, U., Teriaca, L., del Toro Iniesta, J.C., Wimmer-Schweingruber, R.F., Marsch, E., Velli, M., De Groof, A., Walsh, A., Williams, D.: 2020, The Solar Orbiter mission. Science overview. *Astron. Astrophys.* **642**, A1. DOI. ADS.

Ogawara, Y., Takano, T., Kato, T., Kosugi, T., Tsuneta, S., Watanabe, T., Kondo, I., Uchida, Y.: 1991, The SOLAR-A mission – an overview. *Solar Phys.* **136**, 1. DOI. ADS.

Pesnell, W.D., Thompson, B.J., Chamberlin, P.C.: 2012, The Solar Dynamics Observatory (SDO). *Solar Phys.* **275**, 3. DOI. ADS.

Shibata, K., Yokoyama, T.: 2002, A Hertzsprung-Russell-like diagram for solar/stellar flares and corona: emission measure versus temperature diagram. *Astrophys. J.* **577**, 422. DOI. ADS.

Testa, P., Reale, F.: 2020, On the coronal temperature in solar microflares. *Astrophys. J.* **902**, 31. DOI. ADS.

Wright, P.J., Hannah, I.G., Grefenstette, B.W., Glesener, L., Krucker, S., Hudson, H.S., Smith, D.M., Marsh, A.J., White, S.M., Kuhar, M.: 2017, Microflare heating of a solar active region observed with NuSTAR, Hinode/XRT, and SDO/AIA. *Astrophys. J.* **844**, 132. DOI. ADS.



## Authors and Affiliations

**Louise Harra[1,2] · Andrea F. Battaglia[3,2] · Krzysztof Barczynski[1,2] · Hannah Collier[3,2] · Säm Krucker[3,4] · Katharine K. Reeves[5] · George Doschek[6]**

✉ L. Harra
louise.harra@pmodwrc.ch

A.F. Battaglia
andrebat@ethz.ch

K. Barczynski
Krzysztof.Barczynski@pmodwrc.ch

H. Collier
hcollier@ethz.ch

S. Krucker
krucker@berkeley.edu

K.K. Reeves
kreeves@cfa.harvard.edu

G. Doschek
gadoschek@gmail.com

1 Physikalisch-Meteorologisches Observatorium Davos/World Radiation Center (PMOD/WRC), Dorfstrasse 33, 7260 Davos Dorf, Switzerland

2 ETH-Zurich, Honggerberg campus, HIT building, Zurich, Switzerland

3 University of Applied Sciences and Arts Northwestern Switzerland, Bahnhofstrasse 6, 5210 Windisch, Switzerland

4 Space Sciences Laboratory, University of California, 7 Gauss Way, 94720 Berkeley, USA

5 Harvard-Smithsonian Center for Astrophysics, 60 Garden Street, Cambridge, MA 02138, USA

6 Washington DC, USA